Available online at www.sciencedirect.com
ScienceDirect
Journal of the European Ceramic Society 26 (2006) 3613–3620
www.elsevier.com/locate/jeurceramsoc

Composition dependent structure and elasticity of lithium silicate glasses: Effect of ZrO_2 additive and the combination of alkali silicate glasses

Chung-Cherng Lin [a,*], Pouyan Shen [b], H.M. Chang [b], Y.J. Yang [a]

[a] *Institute of Earth Sciences, Academia Sinica, Taipei 115, Taiwan, ROC*
[b] *Institute of Materials Science and Engineering, National Sun Yat-Sen University, Kaohsiung 804, Taiwan, ROC*

Received 1 October 2005; received in revised form 27 December 2005; accepted 6 January 2006
Available online 28 February 2006

Abstract

The elasticity and structure of lithium silicate glasses $Li_2O{\cdot}3SiO_2$, $Li_2O{\cdot}2SiO_2$, and $Li_2O{\cdot}2SiO_2{\cdot}0.135ZrO_2$ were studied at ambient conditions, using both Raman and Brillouin spectroscopies. The conventional nucleating agent, i.e., Zr^{4+} caused a more polymerized silicate network, amorphous phase separation before crystallization, and a significant drop in shear, Young's and bulk moduli, though Raman spectra have revealed that the partial substitution of Zr for Si occurred chiefly in the less polymerized Q^2 species. The compiled data of alkali silicate glasses M_2O–SiO_2 (M = Li, Na, K) showed that each glass displays different M_2O concentrations for getting minimum bulk modulus due to difference in field strength of cations, depolymerization of silicate network, and coordination number of cations. The specific M_2O concentrations for such minima increase with increasing cation size. Different composition dependences of elastic moduli for the glasses having same constituents can be ascribed to different mechanisms for compression and shear deformation.

Keywords: Glass; Mechanical properties; Chemical properties; Spectroscopy; Glass structure

1. Introduction

Lithium monophyllosilicate ($Li_2Si_2O_5$, also known by the wrong name *lithium disilicate*) has been widely used for adherence of ceramics to metals due to its stability below the polymorphism temperature (ca. 930 °C[1]) and beneficial strength at room temperature.[2,3] Lithium metasilicate (Li_2SiO_3) is an alternative for such applications[3] despite of its higher refractive index, slightly larger thermal expansion coefficient and lower strength than $Li_2Si_2O_5$.[1,2,4] The nucleating agent ZrO_2 in silicate glasses[5–7] was known to improve the mechanical properties of the materials due to its martensitic tetragonal-to-monoclinic transformation.[8,9] The ZrO_2 additive was also used to raise the crystallization temperature and the viscosity of Li_2O–SiO_2 glasses,[10] but its effect on the structure and elasticity of the glasses, as of concern to the crystallization path and the mechanical strength of the materials, has not been studied.

Here, Raman and Brillouin spectroscopies were employed to investigate the composition-dependent structure and elasticity of the Li_2O–SiO_2 glasses with/without ZrO_2 addition. Raman spectroscopy is a powerful tool for probing the structure of a glass at molecular level,[11–13] while Brillouin scattering determines the elasticity of glasses.[14,15] A combination of the two techniques in this study showed that the vibrational modes and elastic constants of Li_2O–SiO_2 glasses are fairly correlated analogous to Na_2O–SiO_2 glasses using infrared/Brillouin spectroscopies.[16] To explore the possible rule among alkali silicate glasses, we also compiled the composition dependences of the elastic moduli for three binary alkali silicates glasses. By such comparison, the role of cations on the elastic properties of these glasses can be elucidated.

2. Experimental procedure

Slabs of lithium silicate glasses $L_{14}S_{86}$, $L_{20}S_{80}$ (L and S denote Li_2O and SiO_2, respectively, and the subscripts in weight percent) and $L_{18}S_{72}Z_{10}$ (i.e., $L_{20}S_{80}$ added with 10 wt.%

* Corresponding author. Tel.: +886 2 27839910; fax: +886 2 27839871.

0955-2219/$ – see front matter © 2006 Elsevier Ltd. All rights reserved.
doi:10.1016/j.jeurceramsoc.2006.01.010

ZrO_2) were prepared from powders of SiO_2 (Cerac, 99.9 wt.% pure, 40 mesh), Li_2CO_3 (Cerac, 99.9 wt.% pure, 100 mesh), and ZrO_2 (Gredmann, 99.9 wt.% pure, 325 mesh). The powder batches were ball milled (using alumina balls) in deionized water, oven dried and then melted for 2 h at 1320 °C for $L_{20}S_{80}$ and $L_{18}S_{72}Z_{10}$ and 1445 °C for $L_{14}S_{86}$ in a mullite crucible. The melts were then quenched from a specified temperature (1300 °C) to a copper plate in air. The as-quenched glasses were cut into cubes (1 cm × 1 cm × 1 cm) and then annealed at 400 °C for 4 h to remove residual strain. Fig. 1 shows the differential thermal analysis (DTA, Netzsch 409) traces of the three as-quenched glasses at a heating rate of 10 °C/min in air against alumina reference. The reason for hours annealing at an optimum undercooling with respect to the glass transition temperatures (T_g) (Fig. 1) is to avoid possible devitrification yet ensured relief of the internal strain of the quenched glasses. (In this connection, the Na_2O–SiO_2 and PbO–ZnO–P_2O_5 glasses were reported to relax within several minutes at T_g,[17,18] and 1 h at 300 °C was enough for the stress relief of $3Li_2O{\cdot}7SiO_2$ glass.[19]) Slight amount of Al (ca. 80 ppm) in glasses was detected by Inductively Coupled Plasma (ICP) spectroscopy. Contamination of this level, possibly from the milling balls and crucibles, was assumed to affect little the crystallization behavior and the structure/elasticity of the glasses. All the annealed glasses are homogeneous, transparent, colorless and slightly deliquescent, yet with a few big bubbles ca. hundreds of micrometers in size. Powder X-ray diffraction (Cu Kα) did not detect any crystalline phase in these annealed glasses. Room temperature dwelling for several days in air, however, caused a dissolution/precipitation process to form dendritic crystals near the surface for all samples. These rather minor crystals were either removed or avoided during structure and elasticity characterization at ambient condition by Raman and Brillouin spectroscopies, respectively as addressed in turn.

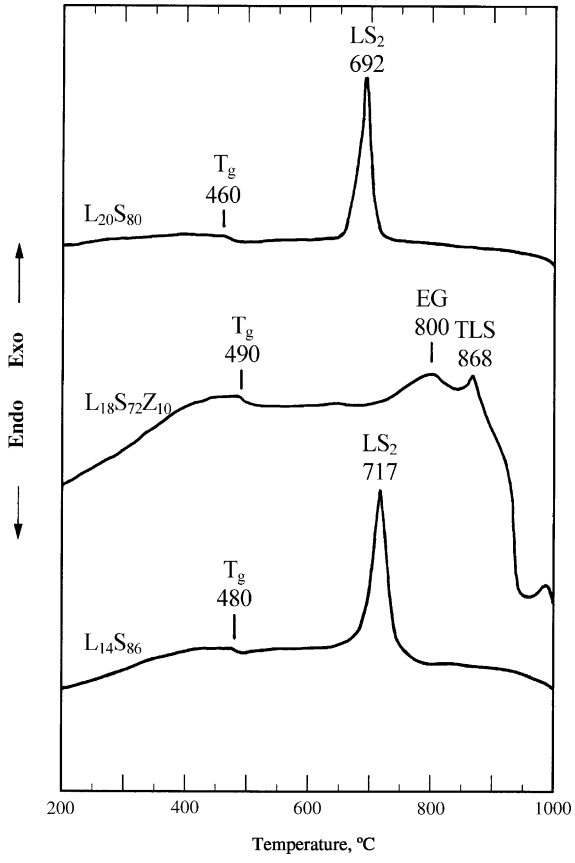

Fig. 1. DTA traces (10 °C/min) of the as-quenched lithium silicate glasses without/with ZrO_2 additive. T_g denotes glass transition temperature. LS_2, EG, and TLS represent crystalline $Li_2Si_2O_5$, eutectic growth of Li_2SiO_3 crystals, and the Li_2SiO_3 to $Li_2Si_2O_5$ transition, respectively.

Raman signals of the as-quenched and annealed glasses were excited by the 514.5-nm line from an argon ion laser (Coherent Innova 90) and collected by a Renishaw-2000 Raman spectroscope under backscattering (180°) geometry and ambient conditions. The spectra were recorded with a Leitz UM32 microscope objective and three accumulations at 30 s integration time with ~120 mW power on the samples. The focused laser spot on samples was estimated to be 2–4 μm in diameter. Wavenumbers are accurate to $\pm 1\ cm^{-1}$ as determined from plasma emission lines. The frequencies and intensities of all Raman bands were estimated based on the possible vibrations and equilibria for silicate anions and the assumption of Gaussian peak profiles for deconvolution of the Raman spectra.

For Brillouin scattering experiments, the annealed glass plates with size of ca. 2 mm × 2 mm and a thickness of ~150 μm were used. The polished opposite faces of the glass plates are parallel to each other within 0.2°. Specimens thus prepared were mounted on a goniometer head of an Eulerian cradle, and then aligned for a symmetric scattering geometry with an external angle of 90° between the incident and scattered beams. With this geometry, the refractive index can be cancelled out in the calculation of acoustic velocity. A 514.5-nm argon ion laser with a temperature-controlled étalon and a six-passes tandem Fabry-Pérot interferometer (JRS Scientific Instruments) were used for the Brillouin experiments at 20 °C. A photomultiplier tube was used as the detector. The free spectral range (FSR) and finesse were 29.9792 GHz and 120, respectively. The laser power on the specimen was about 90 mW. For a 90° symmetric geometry, the acoustic velocity (V) can be calculated by the following formula[20]:

$$V = \frac{\Delta\omega\lambda}{2^{1/2}} \quad (1)$$

where, $\Delta\omega$ is the Brillouin shift, and λ the wavelength of the incident laser. As Raman bands, each Brillouin frequency shift was estimated by assuming the Gaussian peak profiles. In order to obtain better signals, a Glan-Taylor prism was used to rotate the polarization of the incident laser beam to 45°.

The bulk (K), shear (G), and Young's (E) moduli and Poisson's ratios of glasses were calculated based on Brillouin shifts and density (see Ref. 21). However, to eliminate any error caused by density measurements, the densities from Archimedean method have been corrected by the X-ray density of a transparent and pore-free natural quartz single crystal. For Brillouin scattering method, the transit time of the waves is too short to allow exchange of heat. Thus, the entropy is regarded to be constant during measurement, and the moduli obtained from a Brillouin spectrum are all adiabatic. The mechanical strength of a glass

product depends on its elastic constant, shape/architecture, surface/internal defects (e.g., scratches, flaws, bubbles) and the character of the force to which it is subjected. For Brillouin scattering measurement on a small and bubble-free specimen as in the present experiment, the surface defects caused a slightly higher background but no appreciable frequency shift for the signals. Therefore, the present elastic constants/muduli represent the intrinsic and highest strength of the glasses.

3. Results and discussion

3.1. Structure of the present glasses

3.1.1. NBO/T, thermal events and crystallization path

The compositions of the samples used in this study can be represented as $Li_2Si_3O_7$ or $Li_2O{\cdot}3SiO_2$ ($L_{14}S_{86}$), $Li_2Si_2O_5$ or $Li_2O{\cdot}2SiO_2$ ($L_{20}S_{80}$) and $Li_2Si_2O_5{\cdot}0.135\ ZrO_2$ ($L_{18}S_{72}Z_{10}$). Thus, the numbers of non-bridging oxygen per each tetrahedral cation (NBO/T) are 0.67, 1 and 0.937 for $L_{14}S_{86}$, $L_{20}S_{80}$, and $L_{18}S_{72}Z_{10}$, respectively, if Zr^{4+} ion acts as a network former with the assumption of tetrahedral coordination. DTA traces of the glass samples (Fig. 1) showed that the glass transition took place in the range of 460–490 °C. A higher T_g for $L_{14}S_{86}$ than $L_{20}S_{80}$ can be ascribed to more polymerized silicate network (i.e., smaller NBO/T) in the former and thus a higher viscosity. (At the same temperature, viscosity of binary silicate melts and supercooled melts generally decreases with increasing concentration of modifiers and NBO/T.[22]) The addition of 10 wt.% of ZrO_2 to $L_{20}S_{80}$ glass significantly raised T_g, which is consistent with a smaller NBO/T and a higher viscosity as the effect of RO_n addition on Li_2O–SiO_2–RO_n glasses (R = P, V, Zr).[10]

The first crystallization temperatures are 692, 717, and 800 °C for $L_{20}S_{80}$, $L_{14}S_{86}$, and $L_{18}S_{72}Z_{10}$, respectively, and the ZrO_2-free glasses show far sharp exothermic peaks of crystallization (Fig. 1). From stoichiometry viewpoint, a binary silicate glass having M_2O/SiO_2 molar ratio close to or smaller than 1/2, as in the present case, should first crystallize as phyllosilicate (i.e., $Li_2Si_2O_5$) rather than the chain silicate (i.e., Li_2SiO_3). X-ray diffraction analysis showed that $L_{14}S_{86}$ and $L_{20}S_{80}$ were indeed crystallized directly as $Li_2Si_2O_5$ crystals, in consistent with the observations of Freiman and Hench.[23] However, $L_{18}S_{72}Z_{10}$ crystallized initially as Li_2SiO_3 at 800 °C and then $Li_2Si_2O_5$ and zirconia at a higher temperature (868 °C). In other words, the conventional nucleating agent ZrO_2 turned out to suppress the formation of $Li_2Si_2O_5$ crystal unless via the intermediate Li_2SiO_3 at 868 °C. This is surprising because the addition of ZrO_2 to the glass has caused a more polymerized network and may be favored more polymerized species, i.e., $Si_2O_5^{2-}$ rather than $Si_2O_6^{4-}$ according to the present Raman data to be addressed later. Kinser and Hench[19] attributed the crystallization of Li_2SiO_3 at 500 °C to a preexistent phase separation event for the $3Li_2O{\cdot}7SiO_2$ glass with a Li_2O content close to the immiscibility cupola, i.e., ca. 35 mol% Li_2O.[24] The separated glass phases have compositions very close to SiO_2 and $Li_2O{\cdot}2SiO_2$ at 500 °C according to the immiscibility cupola. Therefore, this scenario is difficult, if not impossible, to account for the crystallization of Li_2SiO_3 in glass with a composition close to or inside the immiscibility cupola as the present $L_{18}S_{72}Z_{10}$ at 800 °C and $3Li_2O{\cdot}7SiO_2$ glass at 500 °C. A sufficient low temperature (~500 °C) appeared to be required for Li_2SiO_3 to crystallize in Li_2O–SiO_2 glasses,[19,25] because Li_2SiO_3 did not form in the temperature range of 549–600 °C.[23] Further studies are required to clarify the thermodynamics/kinetics factors for the formation of Li_2SiO_3 in Li_2O–SiO_2 glasses at specified constitutional supercoolings.

3.1.2. Raman bands and Q species

Raman spectra of the as-quenched $Li_2O{\cdot}3SiO_2$, $Li_2O{\cdot}2SiO_2$, and $Li_2O{\cdot}2SiO_2{\cdot}0.135ZrO_2$ glasses are compiled in Fig. 2. Annealing of each glass at a temperature slightly below T_g did not cause appreciable change on Raman spectrum (not shown), indicating that the glass structure remained unchanged from room temperature to T_g. This observation is consistent with the general concept that the structure of a glass at low temperature is identical to its corresponding supercooled melt at T_g.[26–29] Table 1 lists the fitted band frequencies and their assignments for the three glasses according to the method suggested by Mysen et al.[30] It was generally accepted that the basic structure of almost all silicate glasses or melts at one atmospheric pressure can be described by five anionic structural units (the so-called Q species): SiO_4^{4-} (Q^0, monomer), $Si_2O_7^{6-}$ (Q^1, dimer), $Si_2O_6^{4-}$

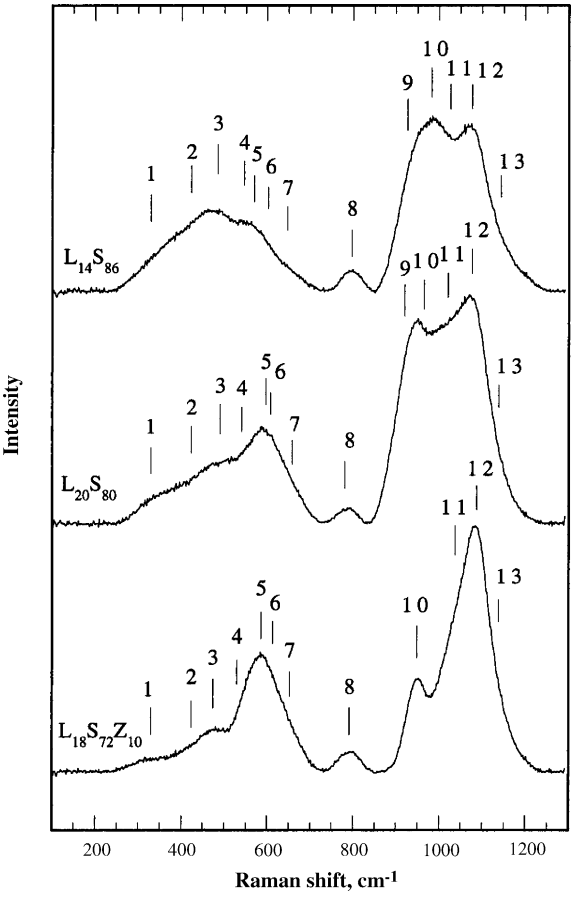

Fig. 2. Raman spectra of lithium silicate glasses without/with ZrO_2 additive. The band numbers are identical with the numbers used in Table 1. Note that the background of each spectrum has been subtracted.

Table 1
Raman frequencies (cm^{-1}) and the assignments for lithium silicate glasses without/with ZrO_2 additive[a]

Band numbers	$L_{14}S_{86}$	$L_{20}S_{80}$	$L_{18}S_{72}Z_{10}$	Assignments
1	329 ± 10 mw	331 ± 8 w	329 ± 5 w	Stretching of cation against oxygen cage[b]
2	425 ± 8 ms	426 ± 10 m	423 ± 7 m	Out-of-plane motion of BO[b,c]
3	485 ± 10 m	490 ± 10 mw	475 ± 10 mw	Rocking of BO[c]
4	548 ± 8 w	543 ± 10 mw	531 ± 10 m	Si–O–Si vibration involving oxygen motion perpendicular to the Si···Si line[b]
5	568 ± 7 m	595 ± 5 mw	585 ± 5 m	Rocking motion of BO in structural units that contain NBO[d]
6	600 ± 10 m	607 ± 10 mw	611 ± 10 mw	Asym Si–O–Si bending of 3-membered siloxane ring of SiO_4[b]
7	648 ± 5 w	659 ± 8 w	650 ± 7 mw	Bending of oxygen in defect structure[c]
8	795 ± 1 mw	783 ± 1 w	791 ± 1 w	Si–O stretching with large Si displacement[b,c]
9	924 ± 3 m	921 ± 4 m		sym stretching of Q^1 ($Si_2O_7^{6}$)[c,e]
10	979 ± 10 s	964 ± 6 s	946 ± 1 m	sym stretching of Q^2 ($Si_2O_6^{4-}$)[c,e]
11	1025 ± 10 m	1022 ± 10 m	1035 ± 7 s	asym stretching of BO in any structural unit[d,f,g]
12	1074 ± 4 s	1079 ± 4 s	1089 ± 3 s	sym stretching of Q^3 ($Si_2O_5^{2-}$)[c,e]
13	1141 ± 15 m	1138 ± 10 mw	1140 ± 8 m	asym stretching of Q^4 [b,c,d]

w = weak, m = medium, mw = medium to weak, ms = medium to strong, s = strong, sym = symmetric, asym = asymmetric, BO = bridging oxygen, NBO = non-bridging oxygen.

[a] The band numbers in column are identical to the numbers used in Fig. 2. The uncertainties were based on three to five fitted data.
[b] McMillan and Wolf.[49]
[c] Mysen et al.[13]
[d] Mysen et al.[52]
[e] Konijnendijk and Stevelts.[31]
[f] Mysen et al.[30]
[g] Galeener.[35]

(Q^2, chain), $Si_2O_5^{2-}$ (Q^3, sheet), and SiO_2 (Q^4, fully polymerized SiO_4 network).[13,31–34] The characteristic Raman signals for the Q species, except Q^4, lie in the range of 850–1100 cm^{-1}. The complicated bands centered at 470–490 cm^{-1} (bands 2–4 in Fig. 2) are the vibrations related to bridging oxygen which is closely related to the extent of polymerization of the silicate network. In addition to difference in frequency, the characteristic Raman bands of Q^4 may be similar to those of amorphous silica which shows two strong bands at 430 and 490 cm^{-1}, four weak bands at ~600, ~800, 1060, and 1176 cm^{-1}.[35]

The Q species of the present glasses would generally follow a disproportionation reaction involved Q^3 and $Q^4 + Q^2$ near T_g due to a NBO/T value of 0.5 ~ 1. However, to get a reasonable fitting, one needs an extra band correlated to Q^1 and thus a secondary equilibrium between Q^2 and $Q^1 + Q^3$ in the two ZrO_2-free glasses. The Raman frequencies of Q species in the more polymerized $L_{14}S_{86}$ glass are slightly higher than those of $L_{20}S_{80}$ glass (Table 1). This is due to that the Raman frequencies of Q species increase with increasing in the extent of polymerization of silicate network as that observed in many glasses and melts.[13,30] However, at the same Li_2O/SiO_2 ratio, the Zr-bearing glass ($L_{18}S_{72}Z_{10}$) shows higher Q^3 and Q^4-related frequencies but lower Q^2 frequency than $L_{20}S_{80}$ (see Table 1). Q^1 unit was not found in $L_{18}S_{72}Z_{10}$ glass. From $L_{20}S_{80}$ to $L_{18}S_{72}Z_{10}$, the intensity ratio between Q^3 and Q^2 bands was increased significantly (see bands 12 and 10 in Fig. 2). In addition, the band involving Si–O stretching with large Si displacement (band 8) in $L_{18}S_{72}Z_{10}$ is more intense than that of $L_{20}S_{80}$. This band is centered at ~800 cm^{-1} for fully polymerized amorphous silica.[35] Therefore, the presence of Zr^{4+} has caused a more polymerized silicate network.

To our knowledge, the effect of Zr^{4+} on Raman spectrum and molecular structure of lithium silicate glass has not been studied. The behavior of TiO_2 in silicate glasses and melts would be useful to our understanding of this issue because both Ti^{4+} and Zr^{4+} have similar chemical properties. In a Raman spectroscopic study, it has been found that Ti^{4+} occurred as discrete units in silicate melts; i.e., Ti^{4+} also formed a set of units similar to the Q species in silicate melts and glasses.[36] Ti^{4+} caused a more polymerized silicate network via the following reaction[36]:

$$\text{Si–O–M–O–Si} + \text{Ti–O–Ti} \leftrightarrow \text{Si–O–Si} + \text{Ti–O–M–O–Ti} \quad (2)$$

where M denotes the metal cation (e.g., Li^+, Na^+). This indicates the presence of amorphous Ti-rich phase in the silicate melts (glasses). The amorphous phase separation caused by TiO_2 additive has been found in other glasses.[37–39] The Raman frequencies for the Ti-bearing units has also been reported elsewhere.[36,37,40] In comparison with Si, Zr has larger cation size (0.59 Å for Zr^{4+} and 0.26 Å for Si^{4+} in coordination number of four[41]) and atomic weight. Assuming that Zr can enter Si position in the Q species, it will cause two consequences: (1) a longer average T–O and M–O bond length (T = Si, Zr, M = Li), and hence lower vibrational frequencies for both M-O-related and Q-species vibrations and (2) weaker Raman intensity due to lowering of polarizability by an increase in average atomic weight. A similar effect of atomic weight on Raman spectrum have also been found in crystalline solids.[42] However, as that mentioned previously, Raman frequency of Q^3 was increased due to the addition of ZrO_2 in $L_{20}S_{80}$ glass, but it is reverse for Q^2 species (Table 1). The frequency change is negligible for the low-frequency bands (bands 2–4) and Q^4-related band (e.g., band 13) in average, though the intensity (peak area) of band 13 increased slightly. Obviously, Zr^{4+} ions prefer to enter in Q^2 species rather than in Q^3 and Q^4, though Zr^{4+} has caused more polymerized network. This case

indicates that Zr^{4+} may cause instability of Q^3 and Q^4 units due to far bigger cation size and much smaller electronegativity than Si^{4+}. Accordingly, a Q^2-based Zr-bearing glassy phase or structural unit (i.e., the Q^2-Zr phase used in the following text) should exist in $L_{18}S_{72}Z_{10}$ glass. This phase should not be as stable as the corresponding Q^2 species due to mismatched cation size in the silicate chain.

Furthermore, if Zr^{4+} also forms a set of discrete units analogous to the case of Ti^{4+}, the Zr-bearing units should show lower-frequency but weaker Raman bands than those of Ti-bearing units at the same coordination due to larger cation size for Zr. However, we were not able to recognize these possible signals from Raman spectrum of $L_{18}S_{72}Z_{10}$ glass (see Fig. 2), though we did not totally exclude the presence of these units (note that the characteristic Raman frequencies for TiO_4^{4-}, Ti_2O6^{4-}, $Ti_2O_5^{2-}$, and TiO_2 (fully polymerized) units are at ~770, 830–850, 870–920, ~930/1100 cm^{-1}, respectively[36]). $L_{20}S_{80}$ glass indeed became more polymerized by the addition of ZrO_2 in view of Raman data and a higher T_g for $L_{18}S_{72}Z_{10}$ glass (see Fig. 1). Zr^{4+} may possibly facilitate polymerization of the silicate phase via a reaction analogous to Eq. (2) for Ti^{4+}-dissolved silicate glasses with Ti^{4+} in coordination number (C.N.) of 4–6. In fact, besides such a polymerized silicate phase and the Q^2-Zr phase, a high C.N. of Zr^{4+}may account for the increase in crosslinking of the glass network. Several studies suggested that the C.N. of Zr^{4+} in silicate and aluminosilicate glasses and/or melts are 5–8 depending on the composition.[39,43–45] Farges et al.[43] pointed out that 6-coordinated Zr^{4+} is stable in deploymerized silicate melts (e.g., NBO/T = 0.29 in alumiosilicate and 0.67 in silicate melts). Thus, Zr^{4+} is likely in octahedral coordination in the present $L_{18}S_{72}Z_{10}$ glass with Li^+ ions as charge-balance ions of ZrO_6. The local environment being different for Si^{4+} and Zr^{4+} also explains the increase of connectivity and T_g in $L_{18}S_{72}Z_{10}$ glass. It should be noted that Zr^{4+}, unlike Ti^{4+}, can interact with silicate units to form the zirconosilicate network in a silicate glass.[39,43,45]

In brief, amorphous phase separation has taken place in $L_{18}S_{72}Z_{10}$ glass before crystallization. At least two amorphous phases exist in $L_{18}S_{72}Z_{10}$ glass: the Q^2-Zr phase and the survived silicate matrix. The Q^2-Zr phase would be the inductor for the first crystallization of Li_2SiO_3 in $L_{18}S_{72}Z_{10}$ glass and the precursor of monoclinic ZrO_2 for annealing $L_{18}S_{72}Z_{10}$ glass at 830–850 °C.[46]

3.2. Elasticity of the present glasses

All the measured elastic constants/moduli fall in the order $L_{20}S_{80} > L_{14}S_{86} > L_{18}S_{72}Z_{10}$ (Table 2). It has been suggested that the elastic constants (moduli) of a glass generally increase with increasing (1) C.N. of the network former cation, (2) degree of network crosslinking, (3) Coulomb contribution of the modifier, and (4) packing density of atoms.[47,48] To explain the observed order, the first two factors can be excluded because a higher C.N. (>4) for Si in oxygen environment is valid only at high pressure[49] and $L_{20}S_{80}$ is less polymerized than $L_{14}S_{86}$. A higher concentration of small-size modifier Li^+ may, however, exert more significant Coulomb contribution to raise elastic constants/moduli as proved experimentally for Li_2O-SiO_2 glasses in the range of 20–35 mol% Li_2O.[16,22,48] A higher glass density due to higher packing density of atoms is also expected to raise elastic constant/moduli. However, the increase of glass density by only 1.6%, whereas shear, bulk, and Young's moduli by 7.6, 26.3, and 10.6%, respectively, from $L_{14}S_{86}$ to $L_{20}S_{80}$, suggests that composition-dependent glass structure needs to be considered as addressed in the following for the compiled alkali-silicate glasses.

Table 2
Density and elastic constants/moduli of lithium silicate glasses (at 20 °C) without/with ZrO_2 additive

Properties	$L_{14}S_{86}$	$L_{20}S_{80}$	$L_{18}S_{72}Z_{10}$
Density (g/cm^3)	2.383	2.419	2.276
C_{11} (GPa)	96.7 ± 0.4	113.5 ± 0.2	89.8 ± 0.3
C_{12} (GPa)	28.4 ± 0.5	40.1 ± 0.2	25.6 ± 0.2
$G = C_{44}$ (GPa) (shear modulus)	34.2 ± 0.1	36.7 ± 0.1	32.1 ± 0.1
Bulk modulus K (GPa)	51.1 ± 0.5	64.6 ± 0.2	47.0 ± 0.2
Young's modulus E (GPa)	83.8 ± 0.1	92.6 ± 0.1	78.4 ± 0.1
Poisson's ratio ν[a]	0.23	0.26	0.22

[a] The uncertainties for all Poisson's ratios are less than 0.003.

Zr^{4+} addition to $L_{20}S_{80}$ glass caused a lower NBO/T value (i.e., more polymerized network) and lower elastic muduli (Table 2), which can be attributed to (1) the formation of a network with weaker T–O bondings (T = Zr, Si) on average because of a relatively large size of Zr^{4+} in oxygen environment, (2) the presence of a Li-depletive ($Li_2O/SiO_2 < 1/2$) residual glass matrix caused by higher-coordinated Zr^{4+} (note that a less Li_2O modifier in a Li_2O–SiO_2 glass lowers elastic moduli, as indicated in Fig. 3 and discussed in the next section) and (3) the formation of interfaces among amorphous phases. A more significant drop of bulk modulus (27%) than shear modulus (13%) (Table 2) implies that the deformation to shearing has been inhibited by the dispersive Zr-bearing phases and/or the interphase interfaces. (Note that gliding of silicate structural units and dispersive phases and elongation of M–O bondings dominates the shear deformation.) The elastic moduli of the ZrO_2-bearing glass may be further affected by the elasticity mismatch across the Zr-bearing phases, as of concern to a Brillouin scattering measurement.

3.3. Composition dependent structure and elasticity of alkali silicate glasses

The compiled alkali silicate glasses showed that both bulk and shear moduli depend on NBO/Si value and alkali content (Fig. 3a and b, respectively). These moduli are from re-calculation of the published adiabatic data based on Brillouin and ultrasonic experiments.[14,22,50] There is a minimum bulk modulus at ~8 mole% Na_2O for Na_2O–SiO_2 glasses (based on the data in Ref. 50) and 15 mol% K_2O for K_2O–SiO_2 glasses (based on the density data listed in Ref. 22 and the Brillouin data in Ref. 14). A hypothetical minimum bulk modulus for Li_2O–SiO_2 glasses is likely near 3 mol% Li_2O as extrapolated from other M_2O–SiO_2 glasses (M = Na, K) assuming positive correlation with M^+ size. There is also likely a minimum for shear modulus

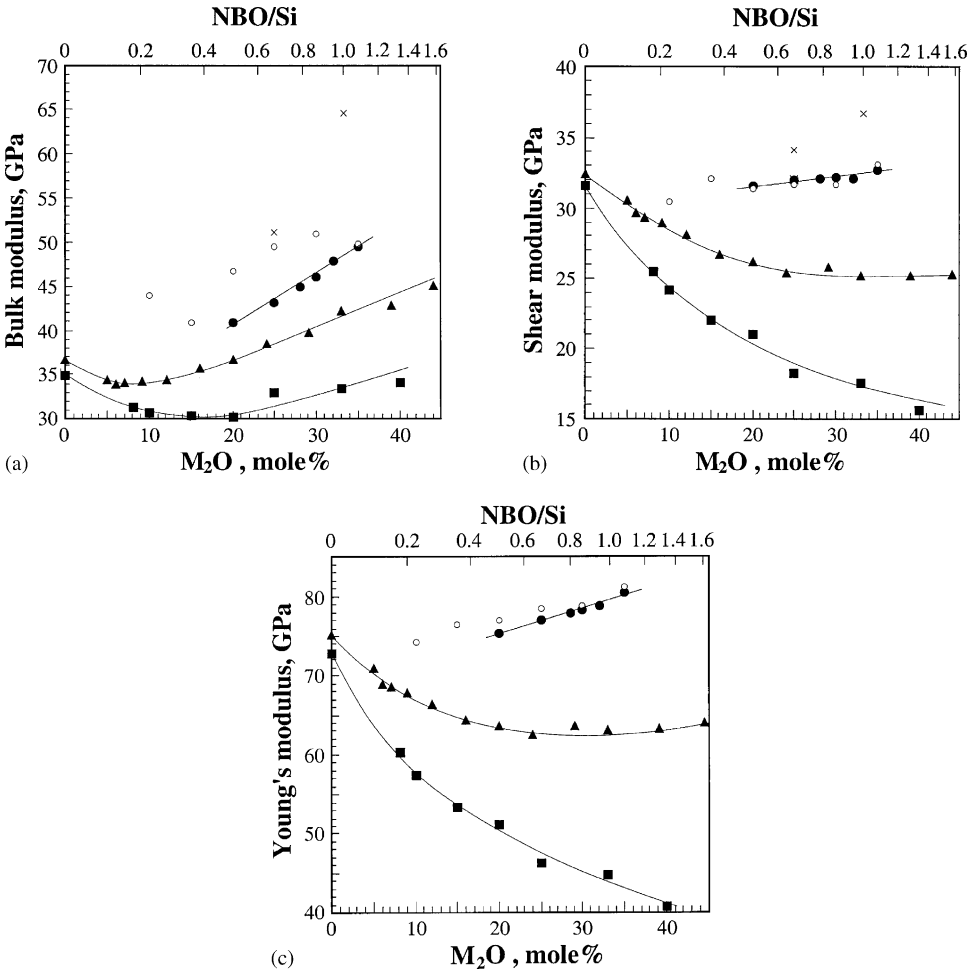

Fig. 3. Variations of (a) bulk, (b) shear, and (c) Young's moduli for binary alkali silicate glasses with NBO/Si and mol% of modifier M_2O (M = Li, Na, K) at ambient conditions. The data of Li_2O–SiO_2 glasses were from this work (denoted as ×) and Bansal and Doremus[22] (● and ○); Na_2O–SiO_2 glasses from Vaills et al.[50] (▲), and K_2O–SiO_2 glasses (■) based on the velocity data in Schroeder et al.[14] and density data in Bansal and Doremus.[22]

versus composition curve, as extrapolated from the composition range reported (Fig. 3b). The Li_2O–SiO_2 glasses have a shear modulus increasing with the increase of Li_2O content up to 35 mol%[22] (Fig. 3b). Linear extrapolation of the shear modulus to zero Li_2O content showed a shear modulus lower than that of amorphous silica. This indicates a minimum shear modulus for Li_2O–SiO_2 glasses estimated to be at ∼10 mol% of Li_2O. Apparently, a minimum shear modulus for Na_2O–SiO_2 glasses may exist by its leveling off above 25 mol% Na_2O (Fig. 3b). However, in a study on the elasticity of $xNa_2O{\cdot}MgO{\cdot}4SiO_2$ glasses, shear modulus of this type of glasses decreases slowly as the equivalent Na_2O mole fraction is increased from 0.33 to 0.60.[51] Relative to Na^+, Mg^{2+} should cause a stronger Coulomb force and thus a more effective strengthening in glass due to higher field strength (Z/r^2, Z = charge, r = ionic radius or M–O distance). This indicates that a minimum shear modulus will not appear in the binary Na_2O–SiO_2 glasses. If field strength of cation (cohesion) is the key factor for strengthening a glass, it is very likely that a minimum shear modulus should not also exist in K_2O–SiO_2 glasses. The monotonical decrease in shear modulus of K_2O–SiO_2 glasses with increasing K_2O content[14] (also see Fig. 3b) is consistent with this inference. The Young's modulus of the three M_2O–SiO_2 glasses (M = Li, Na, K) showed similar composition dependence as the shear modulus. A minimum at about 30 mol% Na_2O (Fig. 3c) seems to occur in Na_2O–SiO_2 glasses. Nevertheless, a minimum Young's modulus was not observed in $xNa_2O{\cdot}MgO{\cdot}4SiO_2$ glasses.[51] Therefore, we conclude both shear and Young's display the similar composition dependences, and the minimum shear and Young's moduli may occur only in Li_2O–SiO_2 glasses. On the basis of the data cited in Fig. 3, Poisson's ratio increases monotonically with the increase of M_2O content, but a minimum Poisson's ratio has not been found for the alkali silicate glasses.

Cation with high Z/r^2 in an amorphous ionic solid tends to cause strong ionic bonding/cohesion although a larger distortion of glass structure due to bending of Si–O–Si angles. With increasing M_2O content, the optimized alkali content for minimum elastic modulus is determined by the competitive factors: strengthening by field strength (cohesion) and weakening by depolymerization of silicate network as that suggested by Vaills et al.[50] for the non-monotonic behavior of C_{11} and C_{44} in Na_2O–SiO_2 glasses. Burkhard[48] attributed the high moduli observed in both Li_2O–SiO_2 and Li_2O–Fe_2O_3–SiO_2 glasses to the bending of Si–O–Si angle caused by the presence of

Li^+ and Fe^{+3}. The Z/r^2 for alkali cations follows the order: $Li^+ > Na^+ > K^+$. This indicates the Li_2O–SiO_2 glass has a least critical alkali concentration or NBO/Si value for a minimum elastic modulus among the alkali-silicate glasses. However, the change in coordination number of cation may contribute to the elastic properties. At the given cation concentration, Mysen et al.[13] found that the average NBO/Si for Q species in Na_2O–SiO_2 melt is smaller than that in BaO–SiO_2 melt. This phenomenon has been attributed to a decrease in average size of Q species with increasing M/Si ratio (M = cation). In the authors' point of view, this case eventually should be attributed to different average C.N. for these cations: a bigger cation has a higher average coordination number which will result in a greater NBO/Si (so, lower Si pack density or a less polymerized network), weaker M–O bond strength and thus lower cohesion. Vaills et al.[50] found that the packing density of Si decreases with the increase of alkali content and cation size due to an increase of the mean distance between the remaining SiO_2 chains. These authors also found the force constants of the cation mode frequencies increase in an order: K < Na < Li.[50] This result is consistent with our inference about the change in C.N. of cations. Therefore, in addition to Z/r^2 and polymerization of network, a difference in average coordination number of cations is also a significant factor for the occurrence of minimum elastic modulus—an increase in C.N. will shift the elasticity minimum to higher M_2O concentration.

The composition dependences and the critical M_2O concentrations for minimum bulk and shear moduli are different for the glasses consisting of the same constituents (cf. Fig. 3). This difference can be attributed to different deformation mechanisms. In fact, shearing involves elongation of Si–O–Si and M–O bondings, gliding between silicate structural units and different glassy phases in a glass. Whereas, compression involves the change in Si–O–Si angles, rotation of SiO_4 groups, shortening of M–O bondings (M = Li, Na, K), and the contraction of both cation and empty polyhedra in/between the silicate structural units. The variation of Young's modulus with M_2O concentration is similar to the trend of shear rather than bulk modulus (cf. Fig. 3b and c) because shear strain rather than normal strain dominates the average strain, as constrained by the elastic constant tensor, for the determination of Young's modulus.

The densities of samples have been corrected in this study. Hence, a higher elastic constant in this study than the ultrasonic values of Li_2O–SiO_2 glasses[22] can be attributed to different methods for measurement of elastic moduli and different content of the Q species caused by different cooling rates. Actually, a slower cooling may result in a denser glass with the amounts of Q species close to their equilibrium values at T_g. Furthermore, impurities and composition inhomogeneity may also cause discrepancies of measurements among various studies. In this concern, slight amount of Al impurities could be introduced in this study during alumina ball milling and later firing in a mullite ($3Al_2O_3{\cdot}2SiO_2$) crucible as mentioned. Foreign Al, if present in considerable amount in lithium silicate glass, would lower Raman frequencies of the Q species. Mysen et al.[52] has pointed out that the stretching frequencies of Q^4 (band 13) and asymmetric stretching of bridging oxygen (band 11) decrease obviously with increasing in concentration of Al, whereas both Q^3 and Q^2 display much insensitive frequency change. However, the large uncertainty for peak fitting has precluded us to do such an analysis at a concentration level as low as ppm. Nevertheless, from the results of Mysen et al. (see Figs. 5, 7 and 9 in Ref. 52), we are sure that the foreign Al and compostion inhomogeneity are not significant enough to affect the structure and elasticity of the present glasses.

4. Conclusions

Combined Raman and Brillouin spectroscopies showed composition dependent structure and elasticity for lithium silicate glasses. The conventional nucleating agent Zr^{4+} in Li_2O–SiO_2 glass has caused a more polymerized silicate network, a significant red shift in Raman frequencies for Q^2 species, and amorphous phase separation before crystallization. Based on Raman spectrum, at least two amorphous phases exist in $L_{18}S_{72}Z_{10}$ glass: the Q^2-Zr phase and the survived silicate matrix. A lower elastic modulus of glass with Zr^{4+} additive can be attributed to a vulnerable network with weaker T–O bondings on average (T = Si, Zr), lower elastic moduli in the residual glass matrix, and the presence of interfaces among amorphous phases. Zr^{4+} addition also changed the crystallization route by forming Li_2SiO_3 intermediate prior to $Li_2Si_2O_5$ crystal. Compiled data of M_2O–SiO_2 glasses (M = Li, Na, K) indicated that there is a minimum bulk modulus in the plots against M_2O concentration. The minimum shear and Young's would exist only in the Li_2O–SiO_2 system. Among the alkali silicate glasses, the critical M_2O concentrations for the minimum bulk modulus increase with the increase of alkali cation size. In addition to the suggested cohesion of cations and depolymerization of network, this phenomenon has been also correlated to a difference in average coordination number of cations. For the glasses consisting of the same constituents, the composition dependences of elastic moduli are different as determined by the structure response to compression and shear deformation.

Acknowledgment

The authors thank the anonymous referee for helpful comments.

References

1. Kalinina, A. M., On the polymorphism of lithium disilicate. *UDC 553.67*, 1970, **541**, 7796–7800.
2. Borom, M. P., Turkalo, A. M. and Doremus, R. H., Strength and microstructure in lithium disilicate glass-ceramics. *J. Am. Ceram. Soc.*, 1975, **58**, 385–391.
3. Beall, G. H. and Duke, D. A., Glass-ceramic technology. In *Glass-Forming Systems (Glass: Science and Technology, Vol. 1)*, ed. D. R. Uhlmann and N. J. Kreidl. Academic Press, New York, 1983, pp. 403–445.
4. Donnay, G. and Donnay, J. D. H., Crystal geometry of some alkali silicates. *Am. Mineral.*, 1953, **38**, 163–171 [and literature cited therein].
5. McMillan, P. W., *Glass Ceramics*. Academic Press, New York, 1979, p. 76.
6. Partridge, G., Nucleation and crystallization phenomena in low expansion Li_2O–Al_2O_3–SiO_2 glass ceramics. *Glass Technol.*, 1982, **23**, 133–138.

7. Strnad, Z., *Glass-Ceramic Materials—Liquid Phase Separation, Nucleation and Crystallization in Glasses*. Elsevier, Amsterdam, 1986, pp. 29–75 [Chapter 2].
8. McCoy, M. A. and Heuer, A. H., Microstructural characterization and fracture toughness of cordierite-ZrO_2 glass-ceramics. *J. Am. Ceram. Soc.*, 1988, **71**, 673–677.
9. Sue, Y. J., Shen, P., Chen, S. Y. and Lu, H. Y., Spherulitic growth from a phase-separated vitreous matrix in a cordierite-Y-stabilized glass ceramic. *J. Am. Ceram. Soc.*, 1991, **74**, 85–91.
10. Matusita, K., Sakka, S., Maki, T. and Tashiro, M., Study on crystallization of glass by differential thermal analysis. Effect of added oxide on crystallization of Li_2O–SiO_2 glasses. *J. Mater. Sci.*, 1975, **10**, 94–100.
11. Konijnendijk, W. L. and Stevelts, J. M., The structure of borate glasses studied by Raman scattering. *J. Non-Cryst. Solids*, 1975, **18**, 307–331.
12. Virgo, D., Mysen, B. O. and Kushiro, I., Anionic constitution of 1-atmosphere silicate melts: implications for the structure of igneous melts. *Science*, 1980, **208**, 1371–1373.
13. Mysen, B. O., Virgo, D. and Scarfe, C. M., Relations between the anionic structure and viscosity of silicate melts—a Raman spectroscopic study. *Am. Mineral.*, 1980, **65**, 690–710.
14. Schroeder, J., Mohr, R., Macedo, P. B. and Montrose, C. J., Rayleigh and Brillouin scattering in K_2O–SiO_2 glasses. *J. Am. Ceram. Soc.*, 1973, **56**, 510–514.
15. Vaills, Y., Luspin, Y., Hauret, G. and Coté, B., Elastic properties of sodium calcium silica glasses by Brillouin scattering. *Solid State Commun.*, 1992, **82**, 221–224.
16. Hauret, G., Vaills, Y., Parot-Rajaona, T., Gervais, F., Mas, D. and Luspin, Y., Dynamic behaviour of $(1–x)SiO_2$–$0.5xM_2O$ glasses (M = Na, Li) investigated by infrared and Brillouin spectroscopies. *J. Non-Cryst. Solids*, 1995, **191**, 85–93.
17. Vaills, Y., Luspin, Y. and Hauret, G., Annealing effects in SiO_2–Na_2O glasses investigated by Brillouin scattering. *J. Non-Cryst. Solids*, 2001, **286**, 224–234.
18. Le Saoût, G., Vaills, Y. and Luspin, Y., Effects of thermal history on mechanical properties of $(PbO)_x(ZnO)_{(0.6-x)}(P_2O_5)_{0.4}$ glasses using Brillouin scattering. *Solid State Commun.*, 2002, **123**, 49–54.
19. Kinser, D. L. and Hench, L. L., Effect of a metastable precipitate on the electrical properties of an Li_2O–SiO_2 glass. *J. Am. Ceram. Soc.*, 1968, **51**, 445–448.
20. Whitfield, C. H., Brody, E. M. and Bassett, W. A., Elastic moduli of NaCl by Brillouin scattering at high pressure in a diamond anvil cell. *Rev. Sci. Instrum.*, 1976, **47**, 942–947.
21. Lin, C. C., Huang, L.-C. and Shen, P., $Na_2CaSi_2O_6$–P_2O_5 based bioactive glasses. I. Elasticity and structure. *J. Non-Cryst. Solids*, 2005, **351**, 3195–3203.
22. Bansal, N. P. and Doremus, R. H., *Handbook of Glass Properties*. Academic Press, San Diego, CA, 1986, pp. 223–336.
23. Freiman, S. W. and Hench, L. L., Kinetics of crystallization in Li_2O–SiO_2 glasses. *J. Am. Ceram. Soc.*, 1968, **51**, 382–387.
24. Filipovich, V. N., Theory of immiscibility. In *Phase Separation in Glass*, ed. O. V. Mazurin and E. A. Porai-Koshits. Elsevier, Amsterdam, 1984, pp. 16–65 [translated by D. D. Petrova, Chapter 2].
25. Kinser, D. L. and Hench, L. L., Hot stage transmission electron microscopy of crystallization in a lithia-silica glass. *J. Mater. Sci.*, 1970, **5**, 369–370.
26. Sweet, J. R. and White, W. B., Study of sodium silicate glasses and liquids by infrared spectroscopy. *Phys. Chem. Glasses*, 1969, **10**, 246–251.
27. Navrotsky, A., Hon, R., Weill, D. F. and Henry, D. J., Thermochemistry of glasses and liquids in the systems $CaMgSi_2O_6$–$CaAl_2Si_2O_8$–$NaAlSi_3O_8$ SiO_2–$CaAl_2Si_2O_8$–$NaAlSi_3O_8$ and SiO_2–Al_2O_3–CaO–Na_2O. *Geochim. Cosmochim. Acta*, 1980, **44**, 1409–1423.
28. Taylor, M., Brown Jr., G. E. and Fenn, P. M., Structure of mineral glasses. III. $NaAlSi_2O_8$ supercooled liquid at 805 °C and the effects of thermal history. *Geochim. Cosmochim. Acta*, 1980, **44**, 109–117.
29. Seifert, F. A., Mysen, B. O. and Virgo, D., Structure similarity of glasses and melts relevant to petrological processes. *Geochim. Cosmochim. Acta*, 1981, **45**, 1879–1884.
30. Mysen, B. O., Finger, L. W., Virgo, D. and Seifert, F., Curve-fitting of Raman spectra of silicate glasses. *Am. Mineral.*, 1982, **67**, 686–695.
31. Konijnendijk, W. L. and Stevelts, J. M., Raman scattering measurements of silicate glasses and compounds. *J. Non-Cryst. Solids*, 1976, **21**, 447–453.
32. Furukawa, T. and White, W. B., Vibrational spectra and glass structure. *J. Non-Cryst. Solids*, 1980, **38/39**, 87–92.
33. Furukawa, T., Fox, K. E. and White, W. B., Raman spectroscopic investigation of the structure of silicate glass. III. Raman intensities and structural units in sodium silicate glasses. *J. Chem. Phys.*, 1981, **75**, 3226–3237.
34. Mysen, B. O., Virgo, D. and Seifert, F., The structure of silicate melts: implication for chemical and physical properties of natural magma. *Rev. Geophys. Space Phys.*, 1982, **20**, 353–383.
35. Galeener, F. L., Band limits and the vibrational spectra of tetrahedral glasses. *Phys. Rev.*, 1981, **B19**, 4292–4297.
36. Mysen, B. O., Ryerson, F. J. and Virgo, D., The influence of TiO_2 on the structure and derivative properties of silicate melts. *Am. Mineral.*, 1980, **65**, 1150–1165.
37. Furukawa, T. and White, W. B., Structure and crystallisation of glasses in the $Li_2Si_2O_5$–TiO_2 system determined by Raman spectroscopy. *Phys. Chem. Glasses*, 1979, **20**, 69–80.
38. de Vekey, R. C. and Majumdar, A. J., The role of TiO_2 in the formation of cordierite glass ceramics. *Phys. Chem. Glasses*, 1975, **16**, 36–43.
39. Galoisy, L., Cormier, L., Rossano, S., Ramos, A., Calas, G., Gaskell, P. and Le Grand, M., Cationic ordering in oxide glasses: the example of transition elements. *Mineral. Mag.*, 2000, **64**, 409–424.
40. Iwamoto, N., Tsunawaki, Y., Fuji, M. and Hatfori, T., Raman spectra of K_2O–SiO_2 and K_2O–SiO_2–TiO_2 glasses. *J. Non-Cryst. Solids*, 1975, **18**, 303–306.
41. Shannon, R. D., Revised effective ionic radii and systematic studies of interatomic distances in halides and chalcogenides. *Acta Cryst.*, 1976, **A32**, 751–767.
42. Lin, C. C., Vibrational spectroscopic study of the system α-Co_2SiO_4–α-Ni_2SiO_4. *J. Solid State Chem.*, 2001, **151**, 102–109.
43. Farges, F., Ponader, C. W. and Brown Jr., G. E., Structural environments of incompatible elements in silicate glass/melt systems. I. Zirconium at trace levels. *Geochim. Cosmochim. Acta*, 1991, **55**, 1563–1574.
44. Galoisy, L., Pélegrin, E., Arrio, M.-A., Ildefonse, P., Calas, G., Ghaleb, D., Fillet, G. and Pacaud, F., Evidence for 6-coordinated zirconium in inactive nuclear waste glasses. *J. Am. Ceram. Soc.*, 1999, **82**, 2219–2224.
45. Calas, G., Cormier, L., Galoisy, L. and Jollivet, P., Structure-property relationships in multicomponent oxide glasses. *C. R. Chimie*, 2002, **5**, 831–843.
46. Chang, H. M., *Crystallization of Li_2O–SiO_2 glass compositions with ZrO_2 addition*. MS thesis, Institute of Materials Science and Engineering, National Sun Yat-Sen University, Taiwan, ROC, 1992.
47. Feltz, A., *Amorphous Inorganic Materials and Glasses*. VCH, Weinheim, Germany, 1993, pp. 113–115.
48. Burkhard, D. J. M., Elastic properties of alkali silicate glasses with iron oxide: relation to glass structure. *Solid State Commun.*, 1997, **101**, 903–907.
49. McMillan, P. F. and Wolf, G. M., Vibrational spectroscopy of silicate liquids. In *Structure, Dynamics and Properties of Silicate Melts*, ed. J. F. Stebbins, P. F. McMillan and D. B. Dingwell. Mineralogical Society of America, Washington, DC, 1995, pp. 247–315 [Chapter 8].
50. Vaills, Y., Luspin, Y. and Hauret, G., Two opposite effects of sodium on elastic constants of silicate binary glasses. *Mater. Sci. Eng.*, 1996, **B40**, 199–202.
51. Li, C. C., *Effects of cation size and anionic structure on the elasticity of alkali and alkaline earth silicate glasses*. MS thesis, Institute of Materials and Mineral Resource Engineering, National Taipei University of Technology, Taiwan, ROC, 2004.
52. Mysen, B. O., Virgo, D. and Kushiro, I., The structural role of aluminum in silicate melts—a Raman spectroscopic study at 1 atmosphere. *Am. Mineral.*, 1981, **66**, 678–701.